Distributed Automatic Load-Frequency Control with Optimality in Power Systems

Xin Chen[1], Changhong Zhao[2], Na Li[1]

***Abstract*— With the increasing penetration of renewable energy resources, power systems face a new challenge in balancing power supply and demand and maintaining the nominal frequency. This paper studies load control to handle this challenge. In particular, a fully distributed automatic load control algorithm, which only needs local measurement and local communication, is proposed. We prove that the control algorithm globally converges to an optimal operating point which minimizes the total disutility of users, restores the nominal frequency and the scheduled tie-line power flows, and respects the thermal constraints of transmission lines. It is also shown that the convergence still holds even when inaccurate system parameters are used in the control algorithm. Lastly, the effectiveness and optimality of the proposed algorithm are demonstrated via numerical simulations.**

I. Introduction

In power systems, generation and load are required to be balanced all the time. Once a mismatch between generation and load occurs, the system frequency will deviate from the nominal value, e.g., 50 Hz or 60 Hz, which may undermine the electric facilities and even cause system collapse. Hence, it is crucial to maintain the frequency closely around its nominal value. Traditionally, the generator-side control [1] plays a dominant role in frequency regulation, where the generation is managed to follow the time-varying load. However, with the deepening integration of renewable energy, it becomes more challenging to maintain the power balance and the nominal frequency due to increased volatility in non-dispatchable renewable generation such as wind and solar.

To address this challenge, load control has received considerable attention in the recent decade as a promising complement to generator control, because controllable loads are ubiquitously distributed in power systems and can respond fast to regulation signals or changes in frequency. There has been a large amount of research effort devoted to frequency regulation provided by controllable loads, including electric vehicles [3], [4], heating, ventilation and air-conditioning systems [5], battery storage systems [6], [7], and thermostatically controlled loads [8]. Several demonstration projects [9]–[11] verified viability of load-side participation in frequency regulation. The literature above focuses on modeling and operating the loads for frequency regulation, and leaves the development of system-wide optimal load control techniques as an unresolved task.

For load-side frequency control, centralized methods [12], [13] have to exchange information over remotely connected control areas, which imposes a heavy communication burden with expanded computational and capacity complexities [14]. This concern motivates a number of studies on distributed control methods. In [15]–[17], load control is implemented by solving a centralized optimization problem using appropriate decomposition methods. The decomposition methods generate optimal control schemes that respect the operational constraints, but their convergence relies on network parameters. In [18], a distributed proportional-integral (PI) load controller is designed to attenuate constant disturbances and improve dynamic performance of the system, whereas operational constraints, such as load power limits and line thermal constraints, are not taken into account. Papers [19]–[21] reversely engineer power system dynamics as primal-dual algorithms to solve optimization problems for load control, and prove global asymptotic stability of the closed-loop system independently of control parameters. However, the scheme in [19] requires the accurate information of power imbalance or generator's shaft angular acceleration, which is hard to obtain in practice. Besides, to implement the scheme in [19], each boundary bus has to communicate with all the other boundary buses within the same control area, which brings heavy remote communication burden if two boundary buses in the same area are far away from each other.

In this paper, we develop an automatic load control (ALC) method for frequency regulation, which can eliminate power imbalance, restore system frequency to the nominal value, and maintain scheduled tie-line power flows in a way that minimizes the total disutility of users for load adjustment. Power system frequency dynamics is interpreted as a primal-dual gradient algorithm that solves a properly formulated optimal load control problem, from which the load control algorithm is extracted. In particular, the proposed ALC method integrates four significant merits: 1) The information of aggregate power imbalance is not required in the control process. 2) With local measurement and local communication, it operates in a fully distributed manner while achieving system-wide optimality. 3) It encodes and satisfies critical operational constraints such as load power limits and line thermal limits. 4) It is globally asymptotically stable even when inaccurate system parameters are used in the controllers. These features overcome the main limitations in the existing approaches reviewed above and facilitate practical implementations of the proposed method.

[1]X. Chen and N. Li are with the School of Engineering and Applied Sciences, Harvard University, USA. chen_xin@g.harvard.edu, nali@seas.harvard.edu.

[2]C. Zhao is with the National Renewable Energy Laboratory, Golden, CO, USA. changhong.zhao@nrel.gov.

The work was supported by NSF 1608509, NSF CAREER 1553407 and ARPA-E through the NODES program.

The remainder of this paper is organized as follows: Section II introduces the power network dynamic model and formulates the optimal load control problem. Section III presents the proposed ALC algorithm, whose convergence to the optimal operating point is analyzed in Section IV. Numerical tests are carried out in Section V, and conclusions are drawn in Section VI.

II. System Model and Problem Formulation

A. Dynamic Network Model

Consider a power network delineated by a graph $G(\mathcal{N}, \mathcal{E})$, where $\mathcal{N} = \{1, \cdots, n\}$ denotes the set of buses and $\mathcal{E} \subset \mathcal{N} \times \mathcal{N}$ denotes the set of transmission lines connecting the buses. Suppose that $G(\mathcal{N}, \mathcal{E})$ is connected and directed, with arbitrary directions assigned to the transmission lines. Note that if $ij \in \mathcal{E}$, then $ji \notin \mathcal{E}$. The buses are divided into two types: generator buses and load buses, which are denoted respectively by the sets $\mathcal{G}$ and $\mathcal{L}$ with $\mathcal{N} = \mathcal{G} \cup \mathcal{L}$. A generator bus is connected to both generators and loads, while a load bus is only connected to loads.

For notational simplicity, all the variables in this paper represent the deviations from their nominal values determined by the previous execution of economic dispatch. We consider the standard direct current (DC) power flow model [22], [23]:

$$P_{ij} = B_{ij}(\theta_i - \theta_j) \qquad \forall ij \in \mathcal{E} \tag{1}$$

where P_{ij} is the active power flow on line ij, B_{ij} is a constant determined by the voltage magnitudes at buses i and j (which are assumed to be constant in the DC model) and the reactance of line ij (which is assumed to be purely inductive in the DC model), and θ_i denotes the voltage phase angle at bus i.

The dynamic model of the power network is:

$$M_i\dot{\omega}_i = -\left(D_i\omega_i + d_i - P_i^{in} + \sum_{j:ij\in\mathcal{E}} P_{ij} - \sum_{k:ki\in\mathcal{E}} P_{ki}\right) \qquad \forall i \in \mathcal{G} \tag{2a}$$

$$0 = D_i\omega_i + d_i - P_i^{in} + \sum_{j:ij\in\mathcal{E}} P_{ij} - \sum_{k:ki\in\mathcal{E}} P_{ki} \qquad \forall i \in \mathcal{L} \tag{2b}$$

$$\dot{P}_{ij} = B_{ij}(\omega_i - \omega_j) \qquad \forall ij \in \mathcal{E} \tag{2c}$$

where ω_i denotes the frequency deviation from the nominal value, M_i is the generator inertia constant, and D_i is the damping coefficient, at bus i. The aggregate power of controllable load at bus i is denoted by d_i, and the difference between the generator mechanical power and the uncontrollable load power at bus i is denoted by P_i^{in}. For load buses $i \in \mathcal{L}$, P_i^{in} represents the minus of the aggregate uncontrollable load power.

Equations (2a) and (2b) describe the frequency dynamics at generator and load buses, respectively. Actually, they both indicate power balance at every time instant of the dynamics, as shown in Figure 1. The damping term $D_i\omega_i = (D_i^g + D_i^l)\omega_i$ characterizes the total effect of generator friction and frequency-sensitive loads, while $P_i^{in} = P_i^g - P_i^l$ captures any change in net uncontrollable power injection. The line flow dynamics is delineated by (2c). The model (2) essentially assumes that the frequency deviation w_i is small at every bus i. See [21] for a justification of the model (2).

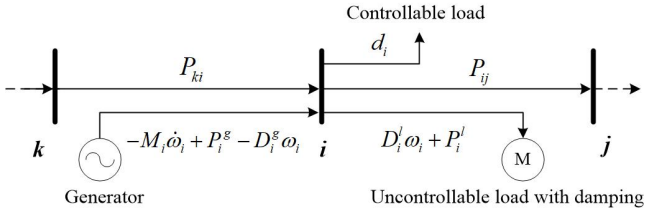

Fig. 1. Frequency dynamics at bus i, where P_i^g and P_i^l denote generator mechanical power and uncontrollable load power, respectively; D_i^g and D_i^l denote the damping coefficients of generators and loads, respectively.

Remark 1. *The simplified linear model* (2) *is for the purpose of algorithm design and stability analysis. The ALC algorithm that will be developed later can be applied to real power systems that have more complex dynamics. In Section V, a high-fidelity power system simulator running a realistic dynamic model is used to test the ALC algorithm.*

B. Optimal Load Control Problem

Consider the scenario when step changes occur in $P^{in} = \left(P_i^{in}\right)_{i\in\mathcal{N}}$. The power imbalance and frequency deviations caused by these step changes will be eliminated through adjustment of controllable loads $d = (d_i)_{i\in\mathcal{N}}$. Our control goals are therefore threefold:

1) Restore the system frequency to its nominal value.
2) Rebalance the system power while making each control area absorb its own power change, so that the scheduled tie-line power transfers are maintained.
3) Modulate the controllable loads in an economically efficient way that minimizes the total disutility for adjusting all the loads, while respecting critical operational constraints including load power limits and line thermal limits.

The second and third control goals can be formulated as the following optimal load control (OLC) problem:

$$\text{Obj.} \ \min_{d,\theta} \quad \sum_{i\in\mathcal{N}} C_i(d_i) \tag{3a}$$

$$\text{s.t.} \ d_i = P_i^{in} - \sum_{j:ij\in\mathcal{E}_{in}} B_{ij}(\theta_i - \theta_j) + \sum_{k:ki\in\mathcal{E}_{in}} B_{ki}(\theta_k - \theta_j) \quad \forall i \in \mathcal{N} \tag{3b}$$

$$\underline{d}_i \le d_i \le \overline{d}_i \qquad \forall i \in \mathcal{N} \tag{3c}$$

$$\underline{P}_{ij} \le B_{ij}(\theta_i - \theta_j) \le \overline{P}_{ij} \qquad \forall ij \in \mathcal{E} \tag{3d}$$

where $\mathcal{E}_{in}$ denotes the subset of lines that connect buses within the same control area. Constants $\overline{d}_i$ and $\underline{d}_i$ are the upper and lower load power limits at bus i, respectively, and $\overline{P}_{ij}$ and $\underline{P}_{ij}$ specify the thermal limits of line ij. The function $C_i(d_i)$ quantifies the cost, or disutility, for

load adjustment d_i. To facilitate the subsequent proof of convergence, we make the following assumptions:

Assumption 1. *For $i \in \mathcal{N}$, the cost function $C_i(\cdot)$ is strictly convex and continuously differentiable.*

Assumption 2. *The OLC problem* (3) *is feasible.*

The objective (3a) is to minimize the total cost of load control. Equation (3b) guarantees that the power imbalance is eliminated *within* each control area; this can be shown by adding (3b) over the buses in the same area $\mathcal{A}$, which leads to $\sum_{i\in\mathcal{A}} d_i = \sum_{i\in\mathcal{A}} P_i^{in}$. Equations (3c) and (3d) impose the load power constraints and the line thermal constraints, respectively. A load control scheme is considered to be optimal if it leads to a steady-state operating point which is a solution to the OLC problem (3).

III. Optimal Automatic Load Control

In this section, a fully distributed automatic load control (ALC) scheme is developed for frequency regulation (see Algorithm 1). The basic approach of controller design is reverse engineering, i.e., to interpret the system dynamics as a primal-dual gradient algorithm to solve the OLC problem (3), which has been used in recent literature [19]–[21].

A. Reformulated Optimal Load Control Problem

To explicitly take into account the first control goal in Section II-B, i.e., frequency regulation, the OLC problem (3) is reformulated as follows:

$$\text{Obj.} \quad \min_{d,\omega,P,\psi} \quad \sum_{i\in\mathcal{N}} C_i(d_i) + \sum_{i\in\mathcal{N}} \frac{1}{2} D_i w_i^2 \tag{4a}$$

$$\text{s.t.} \quad d_i = P_i^{in} - D_i\omega_i - \sum_{j:ij\in\mathcal{E}} P_{ij} + \sum_{k:ki\in\mathcal{E}} P_{ki} \qquad \forall i \in \mathcal{N} \tag{4b}$$

$$\underline{d}_i \le d_i \le \overline{d}_i \qquad \forall i \in \mathcal{N} \tag{4c}$$

$$d_i = P_i^{in} - \sum_{j:ij\in\mathcal{E}_{in}} B_{ij}(\psi_i - \psi_j) + \sum_{k:ki\in\mathcal{E}_{in}} B_{ki}(\psi_k - \psi_i) \qquad \forall i \in \mathcal{N} \tag{4d}$$

$$\underline{P}_{ij} \le B_{ij}(\psi_i - \psi_j) \le \overline{P}_{ij} \qquad \forall ij \in \mathcal{E} \tag{4e}$$

where ψ_i is an auxiliary variable interpreted as the virtual phase angle of bus i, and $\psi_{ij} = B_{ij}(\psi_i - \psi_j)$ is the virtual power flow on line ij; see [19] where the concepts of virtual phase angle and virtual power flow are first proposed. The vectors $\omega := (\omega_i)_{i\in\mathcal{N}}$, $d := (d_i)_{i\in\mathcal{N}}$, $P := (P_{ij})_{ij\in\mathcal{E}}$, and $\psi := (\psi_i)_{i\in\mathcal{N}}$ are defined for notational simplicity.

In the reformulated problem (4), the virtual phase angles ψ and the constraints (4b) and (4d) are introduced so that the primal-dual algorithm of (4) is exactly the power network dynamics under proper control. The equivalence between problems (3) and (4) is established as follows.

Lemma 1. *Let $(\omega^*, d^*, P^*, \psi^*)$ be an optimal solution of problem* (4)*. Then $\omega_i^* = 0$ for all $i \in \mathcal{N}$, and d^* is optimal for problem (3).*

Proof. Let $(\omega^*, d^*, P^*, \psi^*)$ be an optimal solution of (4), and assume that $\omega_i^* \neq 0$ for some $i \in \mathcal{N}$. The optimal objective value of (4) is therefore:

$$f^* = \sum_{i\in\mathcal{N}} C_i(d_i^*) + \sum_{i\in\mathcal{N}} \frac{1}{2} D_i (w_i^*)^2 .$$

Then consider another solution $\{\omega^o, d^*, P^o, \psi^*\}$ with $\omega_i^o = 0$ for $i \in \mathcal{N}$, $P_{ij}^o = B_{ij}(\psi_i^* - \psi_j^*)$ for $ij \in \mathcal{E}_{in}$, and $P_{ij}^o = 0$ for $ij \in \mathcal{E}\backslash\mathcal{E}_{in}$. Obviously, this solution is feasible for problem (4), and its corresponding objective value is

$$f^o = \sum_{i\in\mathcal{N}} C_i(d_i^*) < f^*$$

which contradicts the optimality of $(\omega^*, d^*, P^*, \psi^*)$. Hence $\omega_i^* = 0$ for all $i \in \mathcal{N}$.

Next, note that the constraints (3b) and (4d) take the same form, and that when $\omega = 0$ and given (d, ψ), one can always find P that satisfies (4b) by taking $P_{ij} = B_{ij}(\psi_i - \psi_j)$ for $ij \in \mathcal{E}_{in}$ and $P_{ij} = 0$ for $ij \in \mathcal{E}\backslash\mathcal{E}_{in}$. Therefore the feasible set of (4) restricted to $\omega = 0$ and projected onto the (d, ψ)-space is the same as the feasible set of (3) on the (d, θ)-space. As a result, for any $(\omega^*, d^*, P^*, \psi^*)$ that is an optimal solution of (4), d^* is also optimal for (3). □

B. Automatic Load Control Algorithm

A partial primal-dual gradient method is applied to solve the reformulated OLC problem (4). This solution method can be exactly interpreted as the dynamics of a power network with load-frequency control. Based on this interpretation, an optimal automatic load control (ALC) algorithm is derived.

The Lagrangian function of problem (4) is

$$\begin{aligned}
L =& \sum_{i\in\mathcal{N}} C_i(d_i) + \sum_{i\in\mathcal{N}} \frac{1}{2} D_i w_i^2 \\
&+ \sum_{i\in\mathcal{N}} \lambda_i \left(-d_i + P_i^{in} - D_i\omega_i - \sum_{j:ij\in\mathcal{E}} P_{ij} + \sum_{k:ki\in\mathcal{E}} P_{ki} \right) \\
&+ \sum_{i\in\mathcal{N}} \mu_i \left(-d_i + P_i^{in} - \sum_{j:ij\in\mathcal{E}_{in}} B_{ij}(\psi_i - \psi_j) + \sum_{k:ki\in\mathcal{E}_{in}} B_{ki}(\psi_k - \psi_i) \right) \\
&+ \sum_{ij\in\mathcal{E}_{in}} \sigma_{ij}^+ \left(B_{ij}(\psi_i - \psi_j) - \overline{P}_{ij} \right) \\
&+ \sum_{ij\in\mathcal{E}_{in}} \sigma_{ij}^- \left(-B_{ij}(\psi_i - \psi_j) + \underline{P}_{ij} \right) \\
&+ \sum_{i\in\mathcal{N}} \gamma_i^+ \left(d_i - \overline{d}_i \right) + \sum_{i\in\mathcal{N}} \gamma_i^- \left(-d_i + \underline{d}_i \right)
\end{aligned} \tag{5}$$

where $\lambda_i, \mu_i \in \mathbb{R}$ are the dual variables associated with the equality constraints (4b) and (4d), and $\gamma_i^+, \gamma_i^-, \sigma_{ij}^+, \sigma_{ij}^- \ge 0$ are the dual variables associated with the inequality constraints (4c) and (4e). Define $\lambda_{\mathcal{G}} := (\lambda_i)_{i\in\mathcal{G}}$, $\lambda_{\mathcal{L}} := (\lambda_i)_{i\in\mathcal{L}}$, $\sigma := \left(\sigma_{ij}^+, \sigma_{ij}^-\right)_{ij\in\mathcal{E}_{in}}$, and $\gamma := \left(\gamma_i^+, \gamma_i^-\right)_{i\in\mathcal{N}}$.

A partial primal-dual gradient method is given by the following two steps:

Step 1): Solve for

$$\hat{L}(d,P,\psi,\lambda,\mu,\sigma,\gamma) := \min_{\omega} L(\omega,d,P,\psi,\lambda,\mu,\sigma,\gamma) \tag{6}$$

and then for

$$\overline{L}(d,P,\psi,\lambda_{\mathcal{G}},\mu,\sigma,\gamma) := \min_{\lambda_{\mathcal{L}}} \hat{L}(d,P,\psi,\lambda,\mu,\sigma,\gamma) \tag{7}$$

which leads to:

$$w_i = \lambda_i, \qquad \forall i \in \mathcal{N} \tag{8a}$$

$$0 = P_i^{in} - d_i - D_i\lambda_i - \sum_{j:ij\in\mathcal{E}} P_{ij} + \sum_{k:ki\in\mathcal{E}} P_{ki} \quad \forall i \in \mathcal{L}. \tag{8b}$$

Step 2): The primal-dual gradient algorithm on the rest of variables is:

$$\dot{\lambda}_i = \epsilon_{\lambda_i}\left(P_i^{in} - d_i - D_i\lambda_i - \sum_{j:ij\in\mathcal{E}} P_{ij} + \sum_{k:ki\in\mathcal{E}} P_{ki}\right) \tag{9a}$$

$$\dot{P}_{ij} = \epsilon_{P_{ij}}(\lambda_i - \lambda_j) \tag{9b}$$

$$\dot{d}_i = \epsilon_{d_i}\left(-C_i'(d_i) + \lambda_i + \mu_i - \gamma_i^+ + \gamma_i^-\right) \tag{9c}$$

$$\dot{\psi}_i = \epsilon_{\psi_i}\left[\sum_{j:ij\in\mathcal{E}_{in}} \left(\mu_i - \mu_j - \sigma_{ij}^+ + \sigma_{ij}^-\right) B_{ij} + \sum_{k:ki\in\mathcal{E}_{in}} \left(\mu_i - \mu_k + \sigma_{ki}^+ - \sigma_{ki}^-\right) B_{ki}\right] \tag{9d}$$

$$\dot{\gamma}_i^+ = \epsilon_{\gamma_i^+}\left[d_i - \overline{d}_i\right]_{\gamma_i^+}^+ \tag{9e}$$

$$\dot{\gamma}_i^- = \epsilon_{\gamma_i^-}\left[-d_i + \underline{d}_i\right]_{\gamma_i^-}^+ \tag{9f}$$

$$\dot{\mu}_i = \epsilon_{\mu_i}\left(P_i^{in} - d_i - \sum_{j:ij\in\mathcal{E}_{in}} B_{ij}(\psi_i - \psi_j) + \sum_{k:ki\in\mathcal{E}_{in}} B_{ki}(\psi_k - \psi_i)\right) \tag{9g}$$

$$\dot{\sigma}_{ij}^+ = \epsilon_{\sigma_{ij}^+}\left[B_{ij}(\psi_i - \psi_j) - \overline{P}_{ij}\right]_{\sigma_{ij}^+}^+ \tag{9h}$$

$$\dot{\sigma}_{ij}^- = \epsilon_{\sigma_{ij}^-}\left[-B_{ij}(\psi_i - \psi_j) + \underline{P}_{ij}\right]_{\sigma_{ij}^-}^+ \tag{9i}$$

where (9a) is for $i \in \mathcal{G}$, (9b) is for $ij \in \mathcal{E}$, (9c)–(9g) are for $i \in \mathcal{N}$, and (9h)–(9i) are for $ij \in \mathcal{E}_{in}$. The notations containing ϵ represent arbitrarily selected positive constant step sizes. The operator $[x]_y^+$ means positive projection [24], which equals x if either $x > 0$ or $y > 0$, and 0 otherwise; it ensures $\sigma_{ij}^+, \sigma_{ij}^-, \gamma_i^+, \gamma_i^- \geq 0$.

Since the instant change P_i^{in} of the uncontrollable power injection is usually unknown in practice, a new variable r_i is introduced to substitute μ_i:

$$r_i = \frac{K_i}{\epsilon_{\mu_i}}\mu_i - \frac{K_i}{\epsilon_{\lambda_i}}\lambda_i$$

where K_i is a positive constant. In this way, the necessity to know P_i^{in} is circumvented.

Let $\epsilon_{\lambda_i} = 1/M_i$ and $\epsilon_{P_{ij}} = B_{ij}$. Then the partial primal-dual gradient algorithm (8)–(9) can be equivalently written as the ALC algorithm (10) together with the network dynamics (2). In (10b), μ_i is the abbreviation of the expression $\mu_i = \omega_i \cdot \epsilon_{\mu_i}/\epsilon_{\lambda_i} + r_i \cdot \epsilon_{\mu_i}/K_i$.

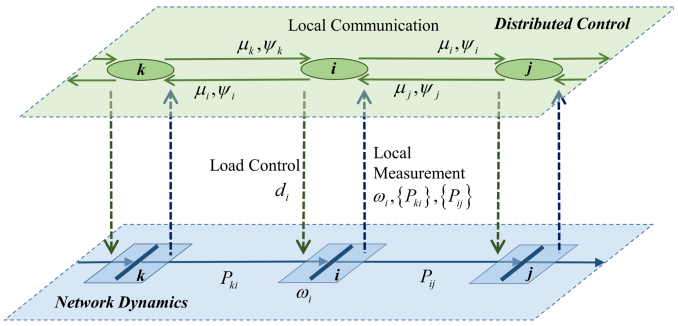

Fig. 2. The automatic load control (ALC) mechanism.

Algorithm 1 Automatic Load Control.

$$\dot{d}_i = \epsilon_{d_i}\left(-C_i'(d_i) + \frac{\epsilon_{\lambda_i} + \epsilon_{\mu_i}}{\epsilon_{\lambda_i}}\omega_i + \frac{\epsilon_{\mu_i}}{K_i}r_i - \gamma_i^+ + \gamma_i^-\right) \tag{10a}$$

$$\dot{\psi}_i = \epsilon_{\psi_i}\left[\sum_{j:ij\in\mathcal{E}_{in}} \left(\mu_i - \mu_j - \sigma_{ij}^+ + \sigma_{ij}^-\right) B_{ij} + \sum_{k:ki\in\mathcal{E}_{in}} \left(\mu_i - \mu_k + \sigma_{ki}^+ - \sigma_{ki}^-\right) B_{ki}\right] \tag{10b}$$

$$\dot{\gamma}_i^+ = \epsilon_{\gamma_i^+}\left[d_i - \overline{d}_i\right]_{\gamma_i^+}^+ \tag{10c}$$

$$\dot{\gamma}_i^- = \epsilon_{\gamma_i^+}\left[-d_i + \underline{d}_i\right]_{\gamma_i^+}^+ \tag{10d}$$

$$\dot{r}_i = K_i\left[D_i\omega_i + \sum_{j:ij\in\mathcal{E}} P_{ij} - \sum_{k:ki\in\mathcal{E}} P_{ki} - \sum_{j:ij\in\mathcal{E}_{in}} B_{ij}(\psi_i - \psi_j) + \sum_{k:ki\in\mathcal{E}_{in}} B_{ki}(\psi_k - \psi_i)\right] \tag{10e}$$

$$\dot{\sigma}_{ij}^+ = \epsilon_{\sigma_{ij}^+}\left[B_{ij}(\psi_i - \psi_j) - \overline{P}_{ij}\right]_{\sigma_{ij}^+}^+ \tag{10f}$$

$$\dot{\sigma}_{ij}^- = \epsilon_{\sigma_{ij}^-}\left[-B_{ij}(\psi_i - \psi_j) + \underline{P}_{ij}\right]_{\sigma_{ij}^-}^+ \tag{10g}$$

The implementation of algorithm (10) is illustrated in Figure 2. In the physical (lower) layer, each bus i measures its own frequency deviation ω_i and the power flows (P_{ki}, P_{ij}) on its adjacent lines. In the cyber (upper) layer, each bus i exchanges the information (μ_i, ψ_i) with its neighboring buses. Then following algorithm (10), each bus i updates

the variables $\psi_i, \gamma_i, \sigma_{ij}, r_i$ and computes its load adjustment d_i. Next, the control command d_i is sent back to the physical layer and executed by the load modulation device. Afterwards, the system frequency and power flows respond to the load adjustment according to the physical law (2). In this manner, the combination of network dynamics (2) and the proposed control algorithm (10) forms a closed loop. In addition, since only local measurement and local communication are required in this process, the proposed ALC algorithm is performed in a fully distributed manner.

Furthermore, the proposed algorithm (10) will converge to a steady-state operating point that is optimal in the sense that it solves the reformulated OLC problem (4). This claim is restated formally as the following theorem.

Theorem 1. *Suppose Assumptions 1 and 2 hold. Then ALC* (10) *together with the power network dynamics* (2) *asympotically converges to a point* $(d^*, \omega^*, P^*, \psi^*, \gamma^*, r^*, \sigma^*)$*, where* $(d^*, \omega^*, P^*, \psi^*)$ *is an optimal solution of problem* (4)*.*

A challenge in implementing (10e) is that the damping coefficient D_i is in general hard to know exactly. It is shown below that the proposed control (10) is robust to inaccuracy in D_i, in the sense that the closed-loop system still converges to an optimal solution of (4), if the inaccuracy in D_i is small enough and some additional conditions are met.

Theorem 2. *Assume the problem* (4) *is feasible and the following conditions are met:*
i) For $i \in \mathcal{N}$*, the cost function* $C_i(d_i)$ *is* α*-strongly convex and second-order continuously differentiable, i.e.,* $C_i \in C^2$ *with* $C_i''(d_i) \geq \alpha > 0$*, in the interior of its domain* $(\underline{d}_i, \overline{d}_i)$*, and* $C_i(d_i) \to +\infty$ *as* $d_i \to \overline{d}_i^-$ *or* $\underline{d}_i^+ \leftarrow d_i$*.*
ii) For $i \in \mathcal{N}$*, the function* C_i' *is Lipschitz continuous with Lipschitz constant* $L > 0$*.*
iii) Infinitely large step sizes ϵ_{d_i} *are used for* (10a)*, which is then reduced to the following algebraic equation:*

$$-C_i'(d_i) + \frac{\epsilon_{\lambda_i} + \epsilon_{\mu_i}}{\epsilon_{\lambda_i}}\omega_i + \frac{\epsilon_{\mu_i}}{K_i} r_i - \gamma_i^+ + \gamma_i^- = 0.$$

iv) An inaccurate $\tilde{D}_i = D_i + \delta a_i$ *is used instead of* D_i *in* (10e)*, and the inaccuracy* δa_i *satisfies:*

$$\delta a_i \in 2\left(\underline{d}' - \sqrt{\underline{d}'^2 + \underline{d}' D_{\min}},\ \underline{d}' + \sqrt{\underline{d}'^2 + \underline{d}' D_{\min}}\right) \quad (11)$$

where $\underline{d}' := 1/L$ *and* $D_{\min} := \min_{i \in \mathcal{N}} D_i$*.*

Then the closed-loop system (2)*,* (10) *converges to a point* $(d^*, \omega^*, P^*, \psi^*, \gamma^*, r^*, \sigma^*)$*, where* $(d^*, \omega^*, P^*, \psi^*)$ *is an optimal solution of* (4)*.*

Remark 2. *The conditions imposed in Theorem 2 are mostly for the purpose of theoretical analysis. That means these conditions are conservative. As we can see in the following section of case studies, the proposed load control algorithm is effective even when the inaccuracy in* D_i *is large.*

The proofs of Theorems 1 and 2 are provided next.

IV. Convergence Analysis

In this section, the proofs of Theorems 1 and 2 are provided as the convergence analysis for the ALC algorithm.

A. Proof of Theorem 1

We prove convergence of the primal-dual gradient algorithm (8)–(9) to an optimal solution of (4), since (8)–(9) are equivalent to the closed-loop system dynamics (2), (10).

The *unique* minimizer ω of L in (6) is obtained by taking

$$\frac{\partial L}{\partial \omega_i} = D_i\omega_i - D_i\lambda_i = 0 \qquad \forall i \in \mathcal{N}$$

which is (8a). Let λ substitute ω in L to obtain $\hat{L}$. The *unique* maximizer $\lambda_{\mathcal{L}}$ of $\hat{L}$ in (7) is obtained by taking

$$\frac{\partial \hat{L}}{\partial \lambda_i} = P_i^{in} - d_i - D_i\lambda_i - \sum_{j:ij\in\mathcal{E}} P_{ij} + \sum_{k:ki\in\mathcal{E}} P_{ki} = 0 \quad \forall i \in \mathcal{L}$$

which is (8b). The resulting minimum value of $\hat{L}$ is denoted by $\overline{L}$, which is a function of $(d, P, \psi, \lambda_{\mathcal{G}}, \mu, \sigma, \gamma)$.

Define $x := (P, \psi)$, $\alpha := (\sigma, \gamma)$, $z := (d, x, \lambda_{\mathcal{G}}, \mu, \alpha)$. Then the primal-dual dynamics (9) can be written as:

$$\begin{aligned} &\dot{d} = -\Xi_d \frac{\partial \overline{L}}{\partial d}, \quad \dot{x} = -\Xi_x \frac{\partial \overline{L}}{\partial x}, \quad \dot{\lambda}_{\mathcal{G}} = \Xi_{\lambda_{\mathcal{G}}} \frac{\partial \overline{L}}{\partial \lambda_{\mathcal{G}}} \\ &\dot{\mu} = \Xi_\mu \frac{\partial \overline{L}}{\partial \mu}, \qquad \dot{\alpha} = \Xi_\alpha \left[\frac{\partial \overline{L}}{\partial \alpha}\right]_\alpha^+ \end{aligned} \quad (12)$$

where $\Xi_d = \mathrm{diag}(\epsilon_{d_i},\ i \in \mathcal{N})$, etc. are diagonal matrices of the positive step sizes. Let $z^* = (d^*, x^*, \lambda_{\mathcal{G}}^*, \mu^*, \alpha^*)$ be any point that makes the right-hand-side of (12) zero, which is called an equilibrium point of (12). Further let $(\omega^*, \lambda_{\mathcal{L}}^*)$ be the solution to (8) given z^*. By Assumptions 1 and 2, strong duality holds for the problem (4), and $(\omega^*, \lambda_{\mathcal{L}}^*, z^*) = (\omega^*, d^*, P^*, \psi^*, \lambda^*, \mu^*, \sigma^*, \gamma^*)$ is a saddle point of L and is primal-dual optimal for (4) [25].

Define the following nonnegative quadratic function of z which is zero at z^*:

$$U_{z^*}(z) := \frac{1}{2}(z - z^*)^T \Xi_z^{-1}(z - z^*) \quad (13)$$

where $\Xi_z := \mathrm{blockdiag}(\Xi_d, \Xi_x, \Xi_{\lambda_{\mathcal{G}}}, \Xi_\mu, \Xi_\alpha)$. The time derivative of U_{z^*} along the trajectory of (12) is:

$$\begin{aligned} \dot{U}_{z^*}(z) = &-(d - d^*)^\top \frac{\partial \overline{L}}{\partial d} - (x - x^*)^\top \frac{\partial \overline{L}}{\partial x} \\ &+ \left(\lambda_{\mathcal{G}} - \lambda_{\mathcal{G}}^*\right)^\top \frac{\partial \overline{L}}{\partial \lambda_{\mathcal{G}}} + (\mu - \mu^*)^\top \frac{\partial \overline{L}}{\partial \mu} \\ &+ (\alpha - \alpha^*)^\top \left[\frac{\partial \overline{L}}{\partial \alpha}\right]_\alpha^+. \end{aligned} \quad (14)$$

It was proved in [19] that

$$(\alpha - \alpha^*)^\top \left[\frac{\partial \overline{L}}{\partial \alpha}\right]_\alpha^+ \leq (\alpha - \alpha^*)^\top \frac{\partial \overline{L}}{\partial \alpha}. \quad (15)$$

In addition, one can show that $\overline{L}$ is strictly convex in d, strictly concave in $\lambda_{\mathcal{G}}$, and linear in the other variables.

Therefore we have:

$$\begin{aligned}\dot{U}_{z^*}(z) \leq\ & \overline{L}\left(d^*, x, \lambda_{\mathcal{G}}, \mu, \alpha\right) - \overline{L}\left(d, x, \lambda_{\mathcal{G}}, \mu, \alpha\right) \\ & + \overline{L}\left(d, x^*, \lambda_{\mathcal{G}}, \mu, \alpha\right) - \overline{L}\left(d, x, \lambda_{\mathcal{G}}, \mu, \alpha\right) \\ & + \overline{L}\left(d, x, \lambda_{\mathcal{G}}, \mu, \alpha\right) - \overline{L}\left(d, x, \lambda_{\mathcal{G}}^*, \mu, \alpha\right) \\ & + \overline{L}\left(d, x, \lambda_{\mathcal{G}}, \mu, \alpha\right) - \overline{L}\left(d, x, \lambda_{\mathcal{G}}, \mu^*, \alpha\right) \\ & + \overline{L}\left(d, x, \lambda_{\mathcal{G}}, \mu, \alpha\right) - \overline{L}\left(d, x, \lambda_{\mathcal{G}}, \mu, \alpha^*\right) \leq 0.\end{aligned} \tag{16}$$

By (16), we have $U_{z^*}(z(t)) \leq U_{z^*}(z(0))$ for all $t \geq 0$. The trajectory $(z(t),\ t \geq 0)$ is therefore bounded since $U_{z^*}(z)$ (13) is radially unbounded. By Lasalle's invariance principle [26], [27], as $t \to +\infty$, the trajectory $z(t)$ approaches a nonempty invariant subset M of the following set:

$$\left\{ z \,\middle|\, \dot{U}_{z^*}(z) \equiv 0 \right\}.$$

By $\dot{U}_{z^*}(z) \equiv 0$ and the invariance of M, one can show that every point $z \in M$ makes the right-hand-side of (12) zero [19]. In other words, M is a set of equilibrium points of (8)–(9), and therefore every point in M is optimal for (4).

Because the trajectory $(z(t),\ t \geq 0)$ is bounded, there exists a subsequence $(z(t_k),\ k \in \mathbb{N})$ that converges to a point $z^0 \in M$ as $k \to +\infty$, and therefore

$$\lim_{k \to +\infty} U_{z^0}\left(z(t_k)\right) = 0.$$

Moreover, $z(t)$ approaches the set where $\dot{U}_{z^0}(z) \equiv 0$ (because the properties of U_{z^*} above hold for any function U_{z^0} where z^0 is an equilibrium of (12)), which implies that

$$\lim_{t \to \infty} U_{z^0}\left(z(t)\right) = C$$

for some constant C. Therefore $C = 0$ and the trajectory $(z(t),\ t \geq 0)$ asymptotically converges to z^0, which is an equilibrium point of (12) and is optimal for (4).

B. Proof of Theorem 2

For $i \in \mathcal{N}$, an inaccurate damping coefficient $\tilde{D}_i = D_i + \delta a_i$ is used instead of D_i in (10e). The closed-loop system (2), (10) is then equivalent to (8)–(9) except that (9g) is now:

$$\begin{aligned}\dot{\mu}_i \ =\ & \epsilon_{\mu_i} \left(P_i^{in} - d_i + \delta a_i \omega_i - \sum_{j:ij \in \mathcal{E}_{in}} B_{ij}\left(\psi_i - \psi_j\right) \right. \\ & \left. + \sum_{k:ki \in \mathcal{E}_{in}} B_{ki}\left(\psi_k - \psi_i\right) \right)\end{aligned} \tag{17}$$

for $i \in \mathcal{N}$, with the additional term $\delta a_i \omega_i$.

By condition i) of Theorem 2, we have that $d_i(t) \in (\underline{d}_i,\ \overline{d}_i)$ if its initial value $d_i(0) \in (\underline{d}_i,\ \overline{d}_i)$, and hence $\gamma_i^+(t) \equiv \gamma_i^-(t) \equiv 0$ for all $t \geq 0$ if their initial values $\gamma_i^+(0) = \gamma_i^-(0) = 0$ for all $i \in \mathcal{N}$. Therefore the dynamics of γ^+ and γ^- can be ignored from (9). Further by condition iii), the control law (9c) is modified to the following:

$$d_i \ =\ \left(C_i'\right)^{-1}\left(\lambda_i + \mu_i\right) \quad \forall i \in \mathcal{N}. \tag{18}$$

Define $(d, \zeta) := (d, x, \lambda_{\mathcal{G}}, \mu, \sigma) = (d, P, \psi, \lambda_{\mathcal{G}}, \mu, \sigma)$ and

$$\tilde{L}(\zeta) := \min_d \overline{L}(d, \zeta)$$

where the minimizer d is given by (18) and satisfies:

$$\frac{\partial \overline{L}}{\partial d}(d, \zeta) = 0.$$

The modified closed-loop system with inaccurate D_i, described by (8), (9a), (9b), (9d), (9h), (9i), (17), (18), can be written as:

$$\begin{aligned}& \dot{x} = -\Xi_x \frac{\partial \tilde{L}}{\partial x}, \quad \dot{\lambda}_{\mathcal{G}} = \Xi_{\lambda_{\mathcal{G}}} \frac{\partial \tilde{L}}{\partial \lambda_{\mathcal{G}}} \\ & \dot{\mu} = \Xi_\mu \left[\frac{\partial \tilde{L}}{\partial \mu} + \delta A \lambda \right], \quad \dot{\sigma} = \Xi_\sigma \left[\frac{\partial \tilde{L}}{\partial \sigma} \right]_\sigma^+\end{aligned} \tag{19}$$

where $\delta A := \mathrm{diag}(\delta a_i,\ i \in \mathcal{N})$. The system (19) can be written more compactly as:

$$\dot{\zeta} \ =\ \Xi_\zeta \left[f(\zeta) \right]_\sigma^+ \tag{20}$$

where $\Xi_\zeta := \mathrm{blockdiag}(\Xi_x, \Xi_{\lambda_{\mathcal{G}}}, \Xi_\mu, \Xi_\sigma)$, and

$$f(\zeta) := \left[-\frac{\partial \tilde{L}}{\partial x}^T, \frac{\partial \tilde{L}}{\partial \lambda_{\mathcal{G}}}^T, \left(\frac{\partial \tilde{L}}{\partial \mu} + \delta A \lambda \right)^T, \frac{\partial \tilde{L}}{\partial \sigma}^T \right]^T.$$

Note that in the vector $\lambda = (\lambda_{\mathcal{L}}, \lambda_{\mathcal{G}})$, only $\lambda_{\mathcal{G}}$ is a variable of the system (19) or (20), whereas $\lambda_{\mathcal{L}}$ is the abbreviation of a vector-valued function $\lambda_{\mathcal{L}}(\zeta)$ defined by the equation:

$$P_i^{in} - d_i(\lambda_i + \mu_i) - D_i \lambda_i - \sum_{j:ij \in \mathcal{E}} P_{ij} + \sum_{k:ki \in \mathcal{E}} P_{ki} = 0,\ \forall i \in \mathcal{L}$$

where $d_i(\lambda_i + \mu_i)$ is defined by (18).

The rest of the proof follows the same technique as the proof of [19, Theorem 15], and therefore we only provide a sketch for it. Consider a Lyapunov function candidate:

$$U(\zeta) = \frac{1}{2}\left(\zeta - \zeta^*\right)^T \Xi_\zeta^{-1}\left(\zeta - \zeta^*\right).$$

We first show that under the dynamics (20), the time derivative of $U(\zeta)$ is upper-bounded by:

$$\dot{U}(\zeta) \leq \int_0^1 (\zeta - \zeta^*)^T [H(\zeta(s))](\zeta - \zeta^*) ds$$

where $\zeta(s) = \zeta^* + s(\zeta - \zeta^*)$, and $H(\zeta)$ is a matrix which is zero everywhere except:
i) a block submatrix corresponding to variables $(P, \mu_{\mathcal{L}})$, which is the same as $H_{P,\lambda_{\mathcal{L}}}(z)$ in [19];
ii) a block submatrix corresponding to variables $(\mu_{\mathcal{G}}, \lambda_{\mathcal{G}})$, which is the same as $H_{\lambda_{\mathcal{G}},\nu_{\mathcal{G}}}(z)$ in [19].

It is shown in [19] that under the condition (11), the matrix $H(\zeta)$ is negative semi-definite. Applying the invariance principle, the convergence result in Theorem 2 can be proved.

Discussions. *Why are γ^+ and γ^- ignored?* If (9e)–(9f) are considered, then instead of proving negative semi-definiteness of the block submatrices corresponding to $(P, \mu_{\mathcal{L}})$ and $(\mu_{\mathcal{G}}, \lambda_{\mathcal{G}})$, we have to prove negative semi-definiteness of the block submatrices corresponding to

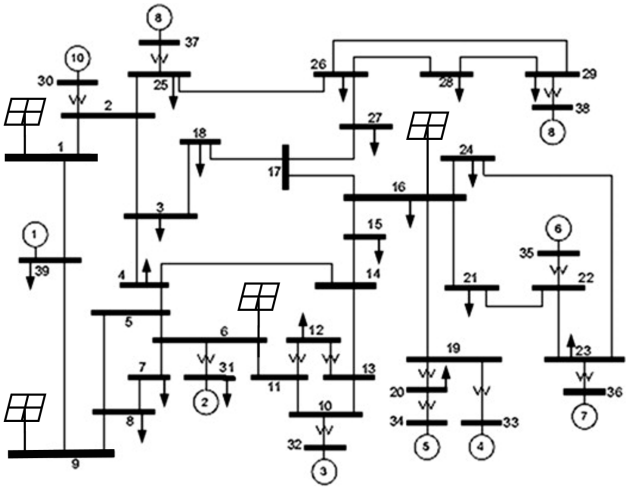

Fig. 3. The 39-bus New England power network.

$(P, \mu_{\mathcal{L}}, \gamma_{\mathcal{L}}^{+}, \gamma_{\mathcal{L}}^{-})$ and $(\mu_{\mathcal{G}}, \lambda_{\mathcal{G}}, \gamma_{\mathcal{G}}^{+}, \gamma_{\mathcal{G}}^{-})$. However, one can show that the latter two larger block submatrices have strictly positive eigenvalues for arbitrarily small δA, which makes the proof technique fail.

Why is the control law modified from the derivative form (9c) *to the stationary form* (18)*?* With the derivative form (9c), one can show that in $H(\zeta)$, the block at the diagonal position corresponding to μ is zero, and hence it is impossible to make $H(\zeta)$ negative semi-definite when the off-diagonal blocks containing δA are non-zero.

V. Case Studies

The effectiveness of the proposed ALC algorithm is demonstrated in numerical simulations. In particular, the performance of ALC under step and continuous power changes is tested, and the impacts of inaccurate damping coefficients and Gaussian noise in local frequency and power flow measurement are studied.

A. Simulation Setup

The 39-bus New England power network in Figure 3 is tested. The simulations are run on Power System Toolbox (PST) [28]. Compared to the analytic model (2), the PST simulation model is more complicated and realistic, which involves the classic two-axis subtransient generator model, the IEEE Type DC1 excitation system model, the alternating current (AC) power flow model, and different types of load models. Detailed configuration and parameters of the simulation model are available online [29].

There are ten generators located at bus-30 to bus-39. To simulate continuous changes in power supply, four photovoltaic (PV) units are added to bus-1, bus-6, bus-9, and bus-16. Bus-1 to bus-29 are load buses with a total active power load of 6.2 GW. Every load bus has an aggregate controllable load, and the disutility function for load control is

$$C_i\left(d_i\right) = c_i \cdot d_i^2$$

where the cost coefficients c_i are set to 1 per unit (p.u.) for bus-1 to bus-5, and 5 p.u. for other load buses. The adjustable load limits are set as $\overline{d}_i = -\underline{d}_i = 0.4$ p.u. with the base power being 100 MVA. In addition, the loads are controlled every 250 ms, which is a realistic estimate of the time-resolution for load control [30]. The damping coefficient D_i of each bus is set to 1 p.u. In the proposed controller, the step sizes ϵ and the constants K_i are all set to 0.5 p.u.

B. Step Power Change

At time $t = 1$ s, step increases of 1 p.u. in load occur at bus-1, bus-6, bus-9, and bus-16. With or without ALC, the system frequency is illustrated in Figure 4. It can be observed that the power network is not capable of bringing the frequency back to the nominal value without ALC. In contrast, the proposed ALC mechanism can restore the system frequency to the nominal value. Figures 5 and 6 present the load adjustments and the total cost of load control under ALC, respectively. It is observed that loads with lower cost coefficients c_i tend to make larger adjustments bounded by their upper limits. This phenomenon indicates that the load adjustments are calculated for system-wide efficiency although the calculations are performed in a distributed way. As a result, the total cost of ALC converges to the minimum of the OLC problem (3) or (4) in the steady state.

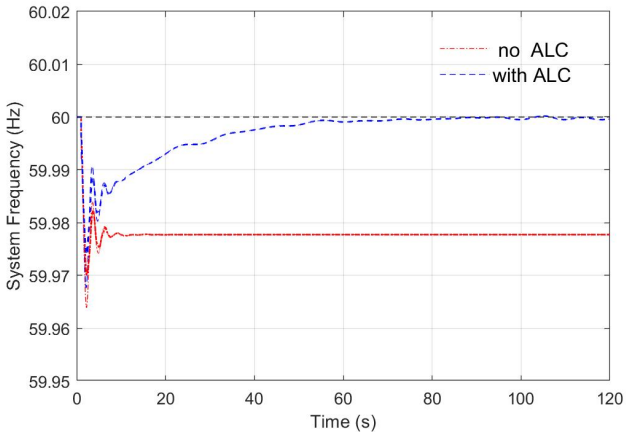

Fig. 4. The frequency dynamics under step power changes.

C. Continuous Power Change

We next study the performance of ALC under continuous power changes. To this end, the PV generation profile of a real power system located within the territory of Southern California Edison is utilized as the power supply of each of the four PV units. The original 6-second data of PV outputs are linearly interpolated to generate power outputs every 0.01 second, which is consistent with the resolution of PST dynamical simulation. The PV power outputs over 10 minutes are shown in Figure 7.

Figures 8 and 9 illustrate the dynamics of system frequency and voltage magnitudes, respectively. It can be observed that ALC can effectively maintain the nominal frequency under time-varying power imbalance. With real-time frequency deviation and power mismatch utilized in the

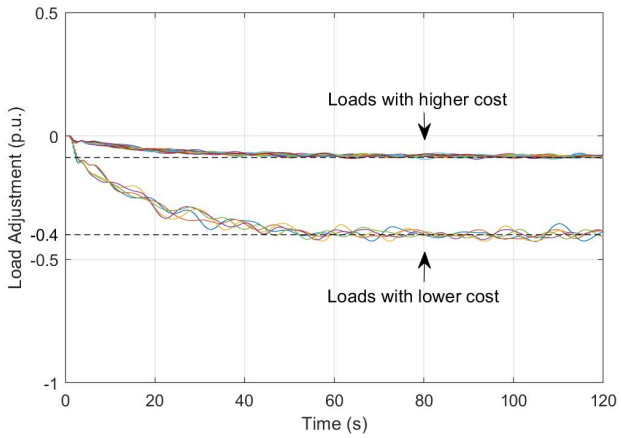

Fig. 5. The load adjustments under ALC.

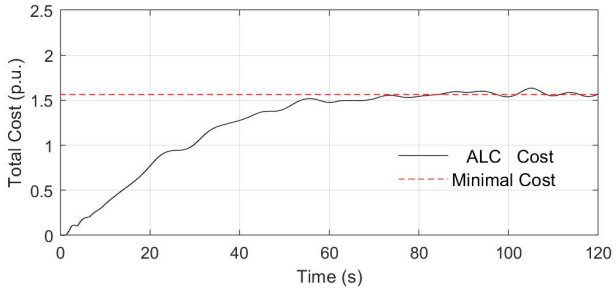

Fig. 6. The trajectory of the total cost of ALC.

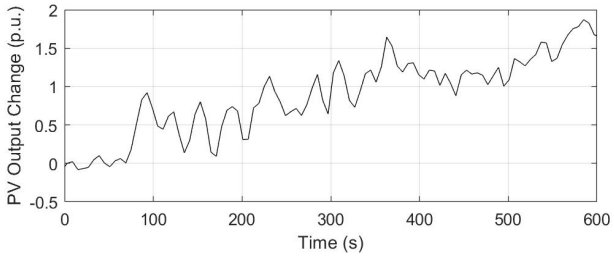

Fig. 7. The PV power outputs.

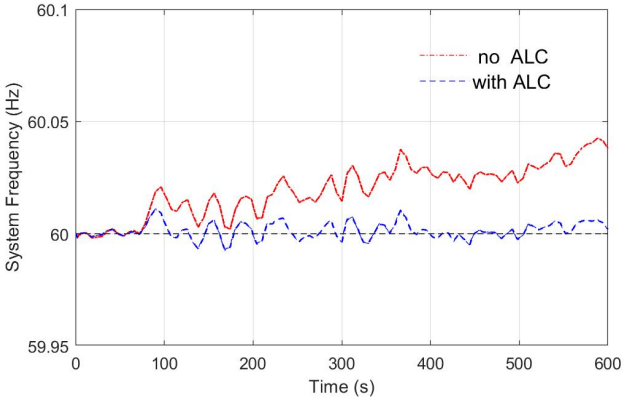

Fig. 8. The frequency dynamics under continuous power changes.

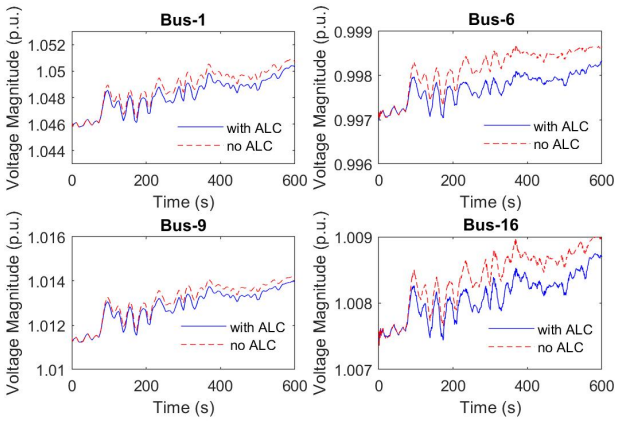

Fig. 9. The dynamics of voltage magnitudes at the PV buses.

control process, ALC can respond promptly to the lasting power fluctuations. Also, from Figure 9, it is observed that the rise in voltage caused by PV generation is alleviated by ALC. The reason is that the power imbalance is absorbed by ubiquitously distributed loads to mitigate the effect of power over-supply on voltage. In summary, the ALC scheme not only maintains system frequency, but also improves the dynamics of voltage magnitudes.

D. Impact of Inaccurate Damping Coefficients

This part is devoted to understanding the impact of inaccurate damping coefficients on the performance of ALC. Let the damping coefficient $\tilde{D}_i$ used by the controller have the following relationship with the accurate D_i:

$$\tilde{D}_i = k \cdot D_i$$

where k is a uniform scaling factor for all the buses $i \in \mathcal{N}$. The factor k is tuned to test the performance of ALC under step power changes. Figure 10 compares the frequency dynamics under ALC with different k.

As shown in Figure 10, the convergence of system frequency becomes slower when smaller damping coefficients are used. As the utilized damping coefficients approach zero, the frequency can be stabilized but cannot be restored to the nominal value. This observation can be explained as follows. When $D_i = 0$, problem (4) imposes no restriction on the system frequency. As a result, only the power imbalance is eliminated, but the frequency cannot be restored. In contrast, when larger damping coefficients are utilized, the convergence of frequency dynamics becomes faster, at the cost of increased oscillations. As the damping coefficients increase to 30 times the actual values, the system frequency becomes unstable. In summary, ALC works well under moderate inaccuracies in the damping coefficients D_i.

E. Impact of Measurement Noise

We now study how the noise in local measurement affects the performance of ALC. Recall that the implementation of ALC relies on local measurement of frequency deviation ω_i and adjacent power flows (P_{ki}, P_{ij}) at every bus $i \in \mathcal{N}$.

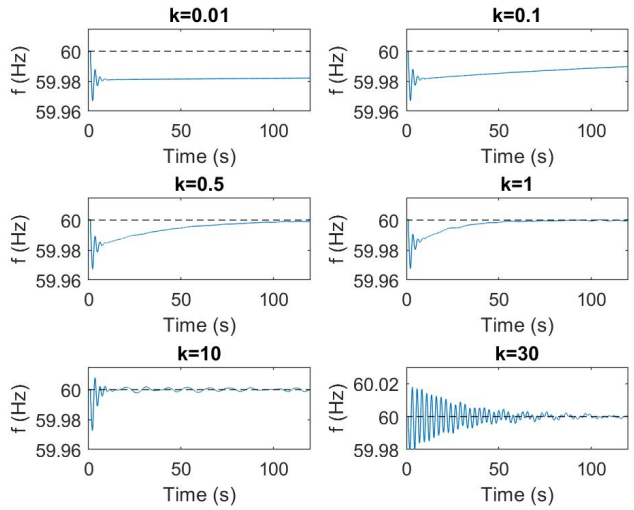

Fig. 10. The frequency dynamics under inaccurate damping coefficients.

First consider the noise ξ_i^ω in the measurement of ω_i, which is assumed to follow Gaussian distribution, i.e., $\xi_i^\omega \sim \mathcal{N}(0, \sigma_\omega^2)$. The measured frequency deviation is thus $\tilde{\omega}_i = \omega_i + \xi_i^\omega$. The standard deviation σ_ω is tuned to test the performance of ALC under step power changes. In the simulations, the noise ξ_i^ω is generated independently over time and across buses, with the Gaussian distribution truncated within the $\pm 3\sigma$ interval to avoid the tail effect. The resultant frequency dynamics is shown in Figure 11.

Next we inject noise ξ_{ij}^P to the measurement of power flow, which also follows the Gaussian distribution, i.e., $\xi_i^P \sim \mathcal{N}(0, \sigma_P^2)$. The frequency dynamics under different levels of such noise is shown in Figure 12.

Figures 11 and 12 show that the system frequency can be restored to the nominal value under measurement noise. Moreover, the frequency presents oscillations that increase with the level of noise.

VI. Conclusion

Based on the reverse engineering approach, we developed a fully distributed automatic load control (ALC) mechanism for frequency regulation in power systems. The combination of ALC and power network dynamics was interpreted as a partial primal-dual gradient algorithm to solve an optimal load control problem. As a result, relying purely on local measurement and local communication, ALC can eliminate power imbalance and restore the nominal frequency with minimum total cost of load adjustment, while respecting operational constraints such as load power limits and line thermal limits. Numerical simulations of the 39-bus New England system showed that ALC can maintain system frequency under step or continuous power changes, and is robust to inaccuracy in damping coefficients as well as measurement noises.

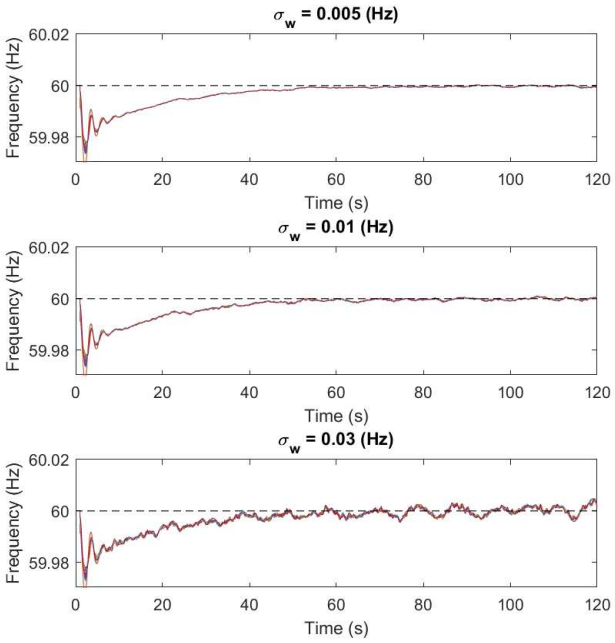

Fig. 11. The frequency dynamics with noise in frequency measurement.

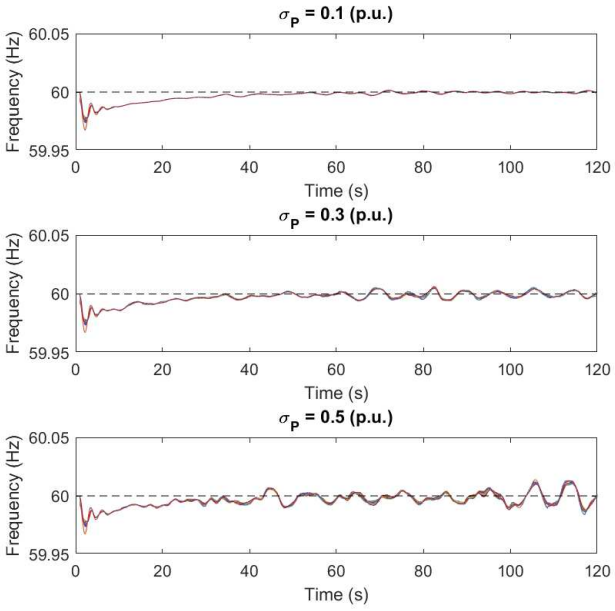

Fig. 12. The frequency dynamics with noise in power flow measurement.

REFERENCES

[1] Y. G. Rebours, D. S. Kirschen, M. Trotignon and S. Rossignol, "A survey of frequency and voltage control ancillary services: Part I: Technical features," *IEEE Trans. Power Syst.*, vol. 22, no. 1, pp. 350-357, Feb. 2007.

[2] B. M. Sanandaji, T. L. Vincent, and K. Poolla, "Ramping rate flexibility of residential HVAC loads," *IEEE Trans. Sustain. Energy*, vol. 7, no. 2, pp. 865-874, Apr. 2016.

[3] H. Liu, Z. Hu, Y. Song, and J. Lin, "Decentralized vehicle-to-grid control for primary frequency regulation considering charging demands," *IEEE Trans. Power Syst.*, vol. 28, no. 3, pp. 3480-3489, Aug. 2013.

[4] H. Liu, J. Qi, J. Wang, P. Li, C. Li and H. Wei, "EV dispatch control for supplementary frequency regulation considering the expectation of EV owners," *IEEE Trans. Smart Grid*, vol. PP, no. 99, pp. 1-1.

[5] I. Beil, I. Hiskens, and S. Backhaus, "Frequency regulation from commercial building HVAC demand response," *Proceedings of the IEEE*, vol. 104, no. 4, pp. 745-757, Apr. 2016.

[6] A. Oudalov, D. Chartouni, and C. Ohler, "Optimizing a battery energy storage system for primary frequency control," *IEEE Trans. Power Syst.*, vol. 22, no. 3, pp. 1259-1266, Aug. 2007.

[7] U. Akram and M. Khalid, "A coordinated frequency regulation framework based on hybrid battery-ultracapacitor energy storage technologies," *IEEE Access*, vol. PP, no. 99, pp. 1-1.

[8] Y. J. Kim, L. K. Norford, and J. L. Kirtley, "Modeling and analysis of a variable speed heat pump for frequency regulation through direct load control," *IEEE Trans. Power Syst.*, vol. 30, no. 1, pp. 397-408, Jan. 2015.

[9] Y. Lin, P. Barooah, S. Meyn, and T. Middelkoop, "Experimental evaluation of frequency regulation from commercial building HVAC systems," *IEEE Trans. Smart Grid*, vol. 6, no. 2, pp. 776-783, Mar. 2015.

[10] G. Heffner, C. Goldman, and M. Kintner-Meyer, "Loads providing ancillary services: review of international experience," Lawrence Berkeley National Laboratory, Berkeley, CA, USA, *Tech. Rep.*, 2007.

[11] D. Hammerstrom et al., "Pacific Northwest GridWise testbed demonstration projects, part II: Grid friendly appliance project," Pacific Northwest Nat. Lab., Richland, WA, USA, *Tech. Rep. PNLL-17079*, Oct. 2007.

[12] M. Aldeen and H. Trinh, "Load frequency control of interconnected power systems via constrained feedback control scheme," *Computers Elect. Engng*, vol. 20, no. 1, pp. 71-88, 1994.

[13] H. Shayeghi, H. Shayanfar, "Application of ANN technique based on μ-synthesis to load frequency control of interconnected power system," *Electr Power Energy Syst*, vol. 28, no. 7, pp. 503-511, Sept. 2006.

[14] A. Pappachen and A. Peer Fathima, "Critical research areas on load frequency control issues in a deregulated power system: A state-of-the-art-of-review," *Renewable Sustain. Energy Reviews*, vol. 72, pp. 163-177, May 2017.

[15] C. Wu and T. Chang, "ADMM approach to asynchronous distributed frequency-based load control," in *Proc. 2016 IEEE Global Conference on Signal and Information Processing (GlobalSIP)*, 2016, pp. 931-935.

[16] S. Abhinav, I. Schizas, F. Ferrese and A. Davoudi, "Optimization-based AC microgrid synchronization," *IEEE Trans. Ind. Informat.*, vol. 13, no. 5, pp. 2339-2349, Oct. 2017.

[17] X. Zhang and A. Papachristodoulou, "A real-time control framework for smart power networks: Design methodology and stability," *Automatica*, vol. 58, pp. 43-50, Aug. 2015.

[18] M. Andreasson, D. V. Dimarogonas, H. Sandberg, and K. H. Johansson, "Distributed control of networked dynamical systems: Static feedback, integral action and consensus," *IEEE Trans. Autom. Control*, vol. 59, no. 7, pp. 1750-1764, Jul. 2014.

[19] E. Mallada, C. Zhao and S. Low, "Optimal load-side control for frequency regulation in smart grids," *IEEE Trans. Autom. Control*, vol. 62, no. 12, pp. 6294-6309, Dec. 2017.

[20] N. Li, C. Zhao, and L. Chen, "Connecting automatic generation control and economic dispatch from an optimization view," *IEEE Trans. Control Netw. Syst.*, vol. 3, no. 3, pp. 254-264, Sept. 2016.

[21] C. Zhao, U. Topcu, N. Li, and S. Low, "Design and stability of load-side primary frequency control in power systems," *IEEE Trans. Autom. Control*, vol. 59, no. 5, pp. 1177-1189, May 2014.

[22] B. Zhang and Y. Zheng, *Advanced Electric Power Network Analysis*, 1st ed. Cengage Learning Asia, Nov. 2010.

[23] B. Stott, J. Jardim, and O. Alsac, "DC power flow revisited," *IEEE Trans. Power Syst.*, vol. 24, no. 3, pp. 1290-1300, Aug. 2009.

[24] D. Feijer and F. Paganini, "Stability of primal-dual gradient dynamics and applications to network optimization", *Automatica*, vol. 46, no. 12, pp. 1974-1981, Dec. 2010.

[25] S. P. Boyd, L. Vandenberghe, Convex Optimization, Cambridge University Press, 2004.

[26] A. Cherukuri, E. Mallada, and J. Corts, "Asymptotic convergence of constrained primal-dual dynamics," *Systems & Control Letters*, vol. 87, pp. 10-15, Jan. 2016.

[27] H. K. Khalil, Nonlinear Systems, 2nd ed. Englewood Cliffs, NJ, USA: Prentice-Hall, 2002.

[28] K. W. Cheung, J. Chow, and G. Rogers, Power System Toolbox ver. 3.0., Rensselaer Polytechnic Institute and Cherry Tree Scientific Software, 2009.

[29] Power System Toolbox Webpage [Online]. Available: `http://www.eps.ee.kth.se/personal/vanfretti/pst/Power_System_Toolbox_Webpage/PST.html`.

[30] P. J. Douglass, R. Garcia-Valle, P. Nyeng, J. stergaard, and M. Togeby, "Smart demand for frequency regulation: Experimental results," *IEEE Trans. Smart Grid*, vol. 4, no. 3, pp. 1713-1720, Sept. 2013.